Entropic Elasticity of Twist-Storing Polymers

J. David Moroz[†] and Philip Nelson[‡]

Department of Physics and Astronomy
University of Pennsylvania
Philadelphia, PA 19104

Abstract

We investigate the statistical mechanics of a torsionally constrained polymer. The polymer is modeled as a fluctuating rod with bend stiffness Ak_BT and twist stiffness Ck_BT. In such a model, thermal bend fluctuations couple geometrically to an applied torque through the relation $Lk = Tw + Wr$. We explore this coupling and find agreement between the predictions of our model and recent experimental results on single λ-DNA molecules. This analysis affords an experimental determination of the microscopic twist stiffness (averaged over a helix repeat). Quantitative agreement between theory and experiment is obtained using $C = 109$ nm (*i.e.* twist rigidity $Ck_BT = 4.5 \times 10^{-19}$ erg cm). The theory further predicts a thermal reduction of the effective twist rigidity induced by bend fluctuations. Finally, we find a small reflection of molecular chirality in the experimental data and interpret it in terms of a twist-stretch coupling of the DNA duplex.
PACS: 87.15.-v, 87.10.+e, 87.15.By.

[†]Address after August 1, 1998: Department of Physics, University of California San Diego 92093 USA
[‡]Corresponding author.

I Introduction

In this paper, we investigate the statistical mechanics of a polymer chain with torsional rigidity. We model the polymer as an elastic rod subject to thermal fluctuations. Each conformation of the chain is statistically weighted according to the energy associated with bending and twisting. This is in contrast to conventional polymer models, which account only for the energy cost of bending the polymer backbone.[1] This neglect of torsional energy is often well justified, as many polymers are free to release twist by swiveling about the single carbon bonds that constitute their backbone. Even for polymers that cannot swivel freely, the twist usually amounts to an uncoupled Gaussian degree of freedom that can simply be integrated away. The situation is quite different, however, in the presence of a torsional constraint. In this case, the twist is coupled to the conformation of the backbone and cannot be eliminated so easily. Such a situation can arise when the polymer is ligated into a circle, or when its ends are clamped and a torque is applied at one end. The concept of a torsional constraint can also be extended to the *dynamics* of a polymer in a viscous fluid: here viscous damping provides the necessary resistance to the stress.[2, 3] Whatever the origin of the constraint, it will result in a coupling between the twist and the bending modes of the backbone.

The origin of this coupling lies in White's theorem: $Lk = Tw + Wr$.[4, 5, 6] This formula relates a global topological invariant of any pair of closed curves (the Linking number, Lk), to the sum of a local strain field (the Twist, Tw) and a global configurational integral (the Writhe, Wr). If the linking number is fixed, the polymer will be forced to distribute the invariant Lk between the degrees of freedom associated with Tw and Wr. From a statistical mechanics point of view, the set of complexions available to the system is then restricted. The elastic energy of each allowed complexion reflects the sum of a twisting energy and a bending energy associated with the Writhe of the backbone. Of course we do not need to consider fixed linking number for torsional rigidity to be important: a chemical potential for Lk in the form of an applied torque also couples the bend fluctuations to the twist.

Perhaps the most important examples of twist-storing polymers are biopolymers, especially DNA. Unlike many of its hydrocarbon-chain cousins, the monomers of DNA are joined by multiple covalent bonds; additional specific pairing interactions between bases prevent slippage between the strands. This multiply-bonded structure inhibits the unwinding of the DNA helix to release a torsional stress; instead, there is an elastic energy cost associated with the deformation.

Recently it has become possible to perform experiments on single molecules of DNA. In a classic experiment, Smith *et al.*[7] anchored one end of a DNA duplex to a solid

substrate while the other end was attached to a magnetic bead. The conformations of the polymer could then be probed by considering the end-to-end extension of the chain as a function of the magnetic force applied to the bead. These experiments, and others which stretch DNA molecules using electric fields,[8] hydrodynamic flows,[9] or optical tweezers[10] were soon analyzed using the "worm-like chain" (WLC) model.[1] Working within this framework, Bustamante, Marko and Siggia[11, 12] and Vologodskii[13] were able to reproduce the experimental force-extension curves for DNA over a wide range of forces (from 10^{-2} pN to 10 pN) with just one fitting parameter, the DNA bend persistence length.

Since the original DNA stretching experiments, significant improvements have been made. In particular, a series of elegant experiments[14, 15, 16] has succeeded in *torsionally* constraining the DNA using swivel-free attachments at both ends. As a result, one can now directly explore the interplay between DNA's internal resistance to twisting and the conformations of its backbone.

In this paper, we will explain some of these new results analytically in terms of a theory of twist-storing polymers. Our final formula, given in (41) below, quantitatively fits the experimental data of Strick *et al.*[14] and of Allemand and Croquette[16] with just two important fit parameters: the bend stiffness A and twist stiffness C (a more precise statement appears below). Our analytical approach rests upon linear elasticity and perturbation theory about a straight rod. Thus we do not address the remarkable structural transitions induced in DNA by torsional stress,[14, 15] nor will we systematically study the plectonemic transition or other phenomena involving self-avoidance. Marko and Siggia have previously studied the effects of thermal fluctuations on plectonemic DNA;[17] we have chosen instead to work in a regime not afflicted by this theoretical difficulty. We will show that our analysis is justified in a well-defined region of parameter space where many experimental data points are available (solid symbols in Figure 1), and from the data deduce the fundamental elastic parameters of DNA.

The main points of our results were announced previously.[18, 19] Some of the steps were independently derived by Bouchiat and Mézard[20] in a different analysis of the same experiments. The present paper gives some new analytical results, particularly in section V.D, and applies the analysis to some new experimental data (see Figure 1).

In addition to these analytical results, Vologodskii and Marko, and Bouchiat and Mézard, have recently performed Monte Carlo simulations[21, 20] to study the conformations of DNA under applied tensions and torques appropriate to those in the experiments studied here. Marko has also studied the related problem of torsional constraints on the overstretching transition.[22, 23]

Apart from quantitatively reproducing the experimental extension curves with just a few fit parameters, our theory also predicts a reduction of the effective twist rigidity of a polymer caused by conformational fluctuations. We give the form of a new effective twist rigidity $C_{\text{eff}} k_{\text{B}} T$, which is smaller than the microscopic rigidity $C k_{\text{B}} T$. This effect, anticipated some time ago by Shimada and Yamakawa[24] has a simple explanation: part of the excess Link imposed on a solid rod can be moved into the bend deformations of its backbone through the coupling associated with the Lk constraint. Our simple formula ((8) below) makes this intuition precise for the case of a highly stretched rod.

It may at first seem that all the relevant physics could be found in the classical works of the nineteenth century,[25] but actually one can see at once that classical beam theory is qualitatively at odds with the experimental data of Figure 1: it says that a rod under tension will simply twist in response to an applied torque τ as long as τ is small enough. Only when the torque exceeds a critical value will the rod buckle into a helical configuration, thus shortening the end-to-end extension. Unlike its macroscopic counterpart, however, a microscopic rod is continuously buffeted by thermal fluctuations. Because the rod is never straight, its average shape will respond as soon as any torsional stress is applied; there is no threshold, as seen in Figure 1. In sections III–V we will create a simple mathematical model embodying this observation and use it to explain the data.

II   Experiment

The statistical mechanical problem of a twist-storing polymer subject to a Lk constraint is realized in the experiments of Strick *et al.*[14, 15] and Allemand and Croquette.[16] In these experiments, a segment of double-stranded λ-DNA of length $L \approx 15.6\,\mu\text{m}$ is held at both ends: one end is fixed to a glass plate while the other is attached to a magnetic bead. Both ends are bound in such a way as to prevent swiveling of the polymer about the point of attachment. By rotating the magnetic bead in an applied magnetic field, the experimenters are then able to adjust the excess linking number to any desired, fixed value.

While the direction of the applied field fixes the linking number, a gradient in the same field allows the DNA molecules to be put under tension. The experiment is therefore able to study the statistical mechanics of the biopolymer in the fixed tension f and linking number Lk ensemble. The measured response is then the end-to-end extension $z(f, Lk)$ of the chain as a function of the applied stress. In contrast, traditional ligation experiments control only L and Lk, and Lk/L can take on only rather widely-spaced discrete values.

Moreover, the measured quantity is gel mobility, whose relation to backbone conformation is not simple.

Some of the experimental results for forces greater than 0.1 pN are shown in Figure 1. In the figure, the solid lines are our theoretical fit to the solid points. These curves were produced by fitting four parameters: the microscopic persistence lengths A, C and twist-stretch coupling D (all averaged over a helical repeat), as well as the arclength of the polymer L. The bend persistence length A has been determined in a number of earlier experiments,[7, 26, 10] while L can be determined from only the data points with zero excess Link. The fitted values of A and L therefore serve mainly as a check of the theory. In our fit we used 69 different points, only some of which are depicted as the solid symbols in Figure 1. The figure also shows open symbols. These points correspond to (f, Lk) pairs that lie outside the region where our model, which has no explicit self-avoidance, is valid. Due to this neglect of self-avoidance, our *phantom chain* model will have a mathematical pathology associated with configurations that include self-crossings. To deal with these difficulties, we will simply require that the chain be pulled hard enough that such configurations become statistically negligible. As we will see, "pulling hard enough" corresponds to a restriction on the applied stretching force f and the applied torque τ (see appendix B). Apart from the restrictions of the *phantom chain* model, there were also omissions of data points for physical reasons. For example, at large applied tensions and torques, the DNA molecule undergoes structural transformations. In section VI, we will discuss our data selection criteria and the fitting procedure more fully.

III   Physical Model

Throughout most of this paper we will model DNA as a fluctuating elastic rod of uniform circular cross-section and fixed contour length L. This idealization neglects DNA's helical nature: in particular, the length scale associated with the helical pitch of the molecule $(2\pi/\omega_0 = 3.6\,\mathrm{nm})$ does not enter as a parameter. The concept of *fractional overtwist* $(\sigma = 2\pi\Delta Lk/L\omega_0)$ is therefore meaningless. Nevertheless, we will retain the traditional notation to provide a connection to the published experimental data, expressing our results in terms of σ and noting that σ and ω_0 enter only in the combination $\sigma\omega_0$. In the main text we will show that our achiral, isotropic elastic rod model captures the main features of Figure 1. At the end of our calculation, in (41), we will also allow for intrinsic stretching and a possible asymmetry between positive and negative σ, a chiral effect associated with the twist-stretch coupling of a helical rod.

In appendix A we will introduce helical pitch effects and show that at modest stretching tension they can be summarized in an effective, "coarse-grained" energy (see (1) below). They also lead to a new phenomenon, *chiral entropic elasticity*, via the twist-bend coupling of DNA.[27] This effect is potentially another source of asymmetry between over- and undertwisting, but the available data do not at present give detailed information about the asymmetry, and so we omit this complication from the main text.

Accordingly we define an elastic energy functional which describes the bending and twisting of an isotropic elastic rod of fixed arclength L:[28]

$$\frac{E_{\text{bend}}}{k_{\text{B}}T} = \frac{A}{2} \int_0^L (\mathrm{d}\hat{t}/\mathrm{d}s)^2 \mathrm{d}s, \qquad \text{and} \qquad \frac{E_{\text{twist}}}{k_{\text{B}}T} = \frac{C}{2} \int_0^L {\Omega_3}^2 \, \mathrm{d}s. \tag{1}$$

In these formulas $\hat{t}(s)$ is the tangent to the rod backbone at the point with arclength s from the end. We imagine inscribing permanently a "material frame" embedded in the rod; then Ω_3 is the rate of rotation of this frame about $\hat{t}$ (see (11) below; our notation mainly follows that of Marko and Siggia[17]). We are free to choose a convenient material frame; we choose one which coincides with the fixed lab frame when the molecule is unstressed. (In keeping with the remarks above, there is no reason to choose a material frame initially rotating relative to the lab at ω_0.) A and C are the bend and twist "persistence lengths," which are given by the respective elastic constants divided by $k_{\text{B}}T$. These parameters are understood to be averaged (or "coarse-grained") over the scale of a helical repeat. In appendix A we find the relation between them and a more elaborate elasticity theory incorporating the intrinsic helicity of the DNA duplex.

Equations (1) are mathematically identical to the *kinetic* energy of a *symmetric spinning top* with arclength s playing the role of time. Hence there is a direct analogy between the dynamical equations of motion for a top and the equations describing the equilibrium for an elastic rod, an observation due to Kirchoff.[29] The main technical point of our analysis is the extension of Kirchoff's observation to a mathematical correspondence between the *thermal fluctuations* of an elastic rod and the *quantum mechanics* of a spinning top.[20, 19, 18]

The bend persistence length A which appears in (1) is a well-known parameter that has been measured in several experiments. Among other things, this parameter is known to depend on the salt concentration of the surrounding fluid.[30] Wang *et al.* have measured $A = 47\,\text{nm}$ for DNA in buffer conditions similar to those in the experiments studied here.[10]

The value of the twist persistence length C has not been determined as directly as A. Cyclization kinetics studies,[31, 32, 24, 33] topoisomer distribution analyses[34, 35] and fluorescence polarization anisotropy (FPA) experiments[36, 37, 38] have provided

5

measurements of this parameter, but these determinations are somewhat indirect and the results have been difficult to reconcile with each other.[30, 39] In particular, results obtained from straight and circular DNA's using a single technique (FPA) yield different values of the twist rigidity: $C \approx 50$ nm for linear DNA's and $C \approx 85$ nm for circular DNA's.[36] This discrepancy may be a consequence of the thermal softening of the torsional rigidity predicted by our theory (see (8)). The main goal of the present paper is to interpret the single DNA molecule data in Figure 1 in terms of a theory we call "torsional directed walks", thereby permitting a new measurement of C. Like the bending rigidity A, C may be expected to depend on the buffer solution; the dependence of C should however be much weaker than A since twisting does not modify the spatial distribution between charges on the backbone to the same degree as bending.

The rod is subject to a stretching force f and a torsional constraint. It will prove simplest to impose the torsional constraint through a fixed applied torque τ rather than directly through a fixed linking number. Since the molecules we will study are many times longer than A or C, we are in the thermodynamic limit, and so we expect the two ensembles to give the same physical results.

The two stresses on the polymer require the introduction of two more terms in the polymer's energy functional:

$$\frac{E_{\text{tension}}}{k_{\text{B}}T} = -\tilde{f} \cdot z = -\tilde{f} \int_0^L \hat{t} \cdot \hat{e}_{\text{z}} \mathrm{d}s, \qquad \text{and} \qquad \frac{E_{\text{torque}}}{k_{\text{B}}T} = -2\pi\tilde{\tau} \cdot Lk. \tag{2}$$

Here z is the end-to-end extension of the polymer. The tension and torque have been expressed in terms of the thermal energy:

$$\tilde{f} \equiv f/k_{\text{B}}T, \quad \text{and} \quad \tilde{\tau} \equiv \tau/k_{\text{B}}T. \tag{3}$$

In (2) and throughout this paper, Lk denotes the *excess* Link, consistent with the remarks at the beginning of this section; thus $Lk = 0$ for the unstressed rod. In general, Lk is defined only for *closed* loops. If we have an *open* chain with both ends held at fixed orientations, as in the experiments under study, then we can draw a fixed, imaginary return path completing our chain to a closed loop and let Lk denote the Link of this closed loop. Choosing the return path so that $Lk = 0$ when the rod is straight and unstressed then gives in general $Lk = Tw + Wr$ where the terms on the right refer only to the open, physical rod.

Before we include E_{torque} in our energy functional, the Link must be more explicitly expressed. To get a useful expression, we first note that the Twist is defined as

$$Tw = \frac{1}{2\pi} \int_0^L \Omega_3 \mathrm{d}s. \tag{4}$$

6

The Writhe involves only the space curve $\vec{r}(s)$ swept out by the rod's centerline. In general, this number is given by a complicated, non-local formula[4, 40, 5] involving a double integral around the closed curve:

$$Wr = \frac{1}{4\pi} \oint \mathrm{d}s \oint \mathrm{d}s' \left(\frac{\mathrm{d}\vec{r}(s)}{\mathrm{d}s} \times \frac{\mathrm{d}\vec{r}(s')}{\mathrm{d}s} \right) \cdot \frac{\vec{r}(s) - \vec{r}(s')}{|\vec{r}(s) - \vec{r}(s')|^3}. \tag{5}$$

However, a result due to Fuller allows us to rewrite this quantity as a single integral over a local Writhe density. This simplification is made possible by noting that for small variations about some reference curve $\vec{r}_0(s)$, the integrand in (5) becomes a total derivative. Performing one of the integrals then yields a single integral over a local quantity.[6] Specializing to the case where the reference curve is just the $\hat{e}_z$-axis then gives[41]

$$Wr = \frac{1}{2\pi} \int \frac{\hat{t} \times \hat{e}_z \cdot \mathrm{d}\hat{t}/\mathrm{d}s}{1 + \hat{t} \cdot \hat{e}_z} \mathrm{d}s. \tag{6}$$

Fuller's result holds as long as there is a continuous set of non-self-intersecting curves interpolating between the reference curve and the curve in question, such that the denominator in (6) never vanishes. We can now combine the terms to get the full energy functional for our model of DNA:

$$\frac{E}{k_B T} = \frac{E_{\mathrm{bend}}}{k_B T} + \frac{E_{\mathrm{twist}}}{k_B T} - \tilde{f} \cdot z - 2\pi\tilde{\tau} \cdot Lk. \tag{7}$$

Formulæ (1,2,4,6, 7) define the elastic model we will use through the end of section V.D. Later, in section VI and appendix A we will consider various elaborations of the model and determine that they are relatively unimportant in capturing the main features of the data in Figure 1.

As noted in the introduction, we expect that thermal fluctuations will have an important effect on the rod's twist degree of freedom. A macroscopic elastic rod under tension will sustain a finite amount of applied torsional stress without buckling. Once a threshold is reached, however, the stress can be partially relaxed by bending the backbone. Linear stability analysis of the energy (7) shows that this threshold is given[25] by $\tilde{\tau}_{\mathrm{crit}} = 2\sqrt{A\tilde{f}}$. Unlike its macroscopic counterpart, however, a microscopic rod is subject to thermal fluctuations. These fluctuations prevent the rod from ever being straight; as we show below, even infinitesimal torsional stresses will then affect the bend fluctuations. Even though there is no chiral energy term, individual fluctuations will not be inversion symmetric. An applied torsion will push the fluctuations with the corresponding helical sense closer to instability, while suppressing those of the opposite helical sense. The end result will be a coupling between the applied torsion and the mean

end-to-end extension of the rod proportional to τ^2 (terms linear in τ must drop out since the model does not break inversion symmetry).

Later we will consider the effects of molecular chirality: *e.g.* in section VI, we will include a twist-stretch coupling term D.[22, 42, 43] It will turn out that the effect of this coupling on the experiment we study is small: this is already apparent in Figure 1 where the data points are nearly symmetric about $\sigma = 0$. Nevertheless, by including the twist-stretch coupling, we will be able to determine the parameter D roughly.

Another way that chirality enters a physical model of DNA is through an anisotropic bending term. Any transverse slice through the molecule is easier to bend in one direction than in another. Microscopically, this anisotropy has its origin in the shape of the base pair plates that make up the rungs on the DNA ladder. Since these plates are longer in one direction than the other, bending about the short axis ("tilt") is more difficult than bending about the long axis ("roll").[44, 45, 46] In appendix A we consider such an anisotropy, as well as the related twist-bend coupling,[27] finding that these effects can be summarized to good accuracy in an effective coarse-grained model of the form (1). This conclusion could have been anticipated since the important fluctuations are on length scales around $2\pi\sqrt{A/\tilde{f}}$, and for the forces below 8 pN that we consider, this averages over at least several helical repeats. We conclude that the treatment of DNA as an achiral rod of elastic material is sufficient to understand how its extension changes under applied tension and torque.

At this point it may be noted that unstressed natural DNA is *not* a perfect helix; its axial symmetry is already broken, even in the absence of thermal fluctuations. In particular, it is well known that the unstressed, zero temperature structure of DNA is sequence dependent.[47, 48] The effect of this quenched disorder has been studied recently by Bensimon, Dohmi, and Mézard[49] and by one of us.[50] For simple models of weak disorder, the main effect is simply to renormalize the bend persistence length A. In the present paper, we neglect explicit inclusion of the quenched disorder associated with sequence-dependent effects. Thus our bend rigidity A is the effective value including disorder.

Even though the bend and twist rigidities represent averages over a helix repeat, they are still microscopic parameters and therefore reflect only the short-scale behavior. As we go to longer length scales, we expect the effective bend and twist rigidities to be modified by the geometric coupling implicit in White's formula. In particular, we will find that the effective twist rigidity is reduced for small applied tensions:

$$C_{\text{eff}} = C\left(1 + \frac{C}{4A\sqrt{A\tilde{f}}}\right)^{-1}. \tag{8}$$

8

The dependence of C_{eff} on length scale enters through $\tilde{f}$: as mentioned above, $\sqrt{A/\tilde{f}}$ sets the scale of the most important fluctuations in the problem. At small tensions, or equivalently at long length scales, C is effectively reduced. Equation (8) describes this "softening" of the twist rigidity. The reducing factor is explicitly dependent on $k_{\text{B}}T$, indicating that this is a thermal effect.

IV Group Language

In the next section we will consider the thermodynamic complexions available to a torsionally constrained polymer. To prepare for the task, we must first define convenient variables for evaluating the energy functional of the last section on the group of rotations, $SO(3)$. The bending and twisting deformations that appear in (1) as well as the Lagrange multiplier terms for extension and Link which appear in (2) will need to be expressed in terms of these variables.

We will use two reference frames related by an element of the rotation group. The first of these frames is "space-fixed"; we will take as its basis the orthonormal triad $\{\hat{e}_i\}$, with $i =$x,y, or z. A rotation $\mathbf{g}(s)$ relates this frame to the "body-fixed" (or "material") frame $\{\hat{E}_\alpha(s)\}$ with $\alpha = 1, 2$, or 3, where s denotes a point on the rod backbone. As mentioned earlier, we will take $\hat{E}_3(s) = \hat{t}(s)$ to be the tangent to the rod's centerline, and the remaining two vectors to be constant directions when the rod is straight and unstressed. The local orientation of the polymer is then given by the 3×3 orthogonal matrix $\mathbf{g}_{\alpha i}(s) = \hat{E}_\alpha(s) \cdot \hat{e}_i$. The matrix $\mathbf{g}$ contains only three independent entries. We will sometimes find it convenient to represent it in a nonredundant way using Euler angles:

$$\mathbf{g}(s) \;\; = \;\; \mathrm{e}^{-\mathsf{L}_3\psi(s)}\mathrm{e}^{-\mathsf{L}_1\theta(s)}\mathrm{e}^{-\mathsf{L}_3\phi(s)}. \tag{9}$$

Thus for example $\hat{t}(s) \cdot \hat{e}_{\text{z}} = \mathbf{g}_{3\text{z}}(s) = \cos\theta(s)$.

The generators of infinitesimal rotations are then matrix operators acting on $\mathbf{g}$. When these operators act from the left they are called "body-fixed rotations"; when they act from the right they are called "space-fixed rotations". In either case a convenient basis for the generators is

$$\mathsf{L}_1 = \begin{pmatrix} 0 & 0 & 0 \\ 0 & 0 & 1 \\ 0 & -1 & 0 \end{pmatrix}, \qquad \mathsf{L}_2 = \begin{pmatrix} 0 & 0 & -1 \\ 0 & 0 & 0 \\ 1 & 0 & 0 \end{pmatrix}, \qquad \text{and} \qquad \mathsf{L}_3 = \begin{pmatrix} 0 & 1 & 0 \\ -1 & 0 & 0 \\ 0 & 0 & 0 \end{pmatrix}. \tag{10}$$

We can then describe the rotation of the material frame as we walk along the rod backbone as an infinitesimal body-fixed rotation Ω or as a space-fixed rotation $\hat{\Omega}$, where

$$\Omega = \dot{\mathbf{g}}\mathbf{g}^{-1} \quad \text{and} \quad \hat{\Omega} = \mathbf{g}^{-1}\dot{\mathbf{g}}. \tag{11}$$

9

Here and elsewhere, a dot signifies $\mathrm{d}/\mathrm{d}s$. We will also write the projections of the rotation rates onto the generators as

$$\Omega_\alpha \equiv (\Omega, \mathsf{L}_\alpha) \equiv -\frac{1}{2}\mathrm{Tr}\,[\Omega \mathsf{L}_\alpha] \tag{12}$$

and similarly for $\hat{\Omega}_i$.

With these definitions we can cast the formulas of the previous section into more useful forms. We first compute that $(\mathrm{d}\hat{t}/\mathrm{d}s)^2 = \Omega_1{}^2 + \Omega_2{}^2$ and substitute into (1). Next, a simple calculation gives

$$\Omega_3 = -(\dot{\psi} + \cos\theta\dot{\phi}) \quad\text{and}\quad \hat{\Omega}_z = -(\dot{\phi} + \cos\theta\dot{\psi}). \tag{13}$$

Next, note that $\hat{t} = \hat{E}_3 = \mathsf{g}_{3i}\hat{e}_i = \sin\theta(\sin\phi\hat{e}_x + \cos\phi\hat{e}_y) + \cos\theta\hat{e}_z$. Explicit evaluation of the local Writhe density (6) then gives with (4,13) that

$$Lk = -\frac{1}{2\pi}\int(\dot{\psi} + \dot{\phi})\,\mathrm{d}s = \frac{1}{2\pi}\int\frac{\Omega_3 + \hat{\Omega}_z}{1 + \cos\theta}\,\mathrm{d}s. \tag{14}$$

With this last expression, the energy functional (7) is explicitly given in terms of an element of the rotation group and its derivatives, as expressed by the angular frequencies $\Omega_{=\alpha}$ and Ω_z.

We close this section with a mathematical fine point, which will not affect our calculation. Strictly speaking, our configuration space is only locally the group manifold $SO(3)$. We will exclude the points $\theta = \pi$ where (14) is singular. Moreover, we need to "unwrap" the remaining space. The physical origin of this step is simply the fact that rotating the rod by 2π does not return it to an equivalent state, but rather introduces an extra unit of Link. Mathematically we simply remember that $\phi + \psi$ is not to be identified modulo 2π (see (14)), though $\phi - \psi$ is.

V   Calculation

V.A   The Path Integral

We wish to compute the average extension $\langle z \rangle$ and relative excess Link $\langle Lk \rangle$ for a twist-storing polymer subject to a given tension and torque. To find these properties, we must first compute the partition function. At each point along the arclength of the polymer, the local orientation will be given by some rotation g. To calculate the weight of any configuration entering into the partition function, we simply apply the appropriate Boltzmann factor. In the last section we described how the terms of the energy functional

appearing in this factor can be written in terms of rotations. Using these expressions, it is now possible to write down a path integral on the group space:

$$\mathcal{Z} = \int [d\mathbf{g}(s)] \, \exp\left(-\frac{1}{k_B T}\left(E_{\text{bend}} + E_{\text{twist}}\right) + 2\pi\tilde{\tau}\cdot Lk + \tilde{f}\cdot z\right). \qquad (15)$$

This partition function gives us the quantities of interest, namely the average chain extension $\langle z \rangle$ and the average excess Link resulting from an applied tension and torque:

$$\langle z \rangle = \left.\frac{\partial}{\partial \tilde{f}}\right|_{\tilde{\tau}} \ln\mathcal{Z}, \qquad \langle Lk \rangle = \left.\frac{1}{2\pi}\frac{\partial}{\partial\tilde{\tau}}\right|_{\tilde{f}} \ln\mathcal{Z}. \qquad (16)$$

A direct evaluation of the partition sum in (15) is difficult; fortunately, such an evaluation proves to be unnecessary. In this paper we instead extend a standard polymer physics trick.[1, 12] It turns out that the partition sum is closely related to the "propagator" for the probability distribution for the polymer's orientation $\mathbf{g}$. We define the unnormalized propagator by

$$\Psi(\mathbf{g}_f, s_f; \mathbf{g}_i, s_i) = \int_{\substack{\mathbf{g}(s_f)=\mathbf{g}_f \\ \mathbf{g}(s_i)=\mathbf{g}_i}} [d\mathbf{g}(s)] \, \exp\left(-\frac{E[\mathbf{g}(s)]}{k_B T}\right). \qquad (17)$$

The probability $P_s(\mathbf{g})$ for the polymer to have orientation $\mathbf{g}$ at position s is then given by a multiplicative constant times $\int d\mathbf{g}_i \, \Psi(\mathbf{g}, s; \mathbf{g}_i, 0)P_{s=0}(\mathbf{g}_i)$. More interestingly from our perspective, for a long chain $\log\Psi(\mathbf{g}, L; \mathbf{g}_i, 0)$ becomes independent of $\mathbf{g}$ and $\mathbf{g}_i$. In fact the propagator is then just a constant times the partition function $\mathcal{Z}$. The utility of studying the seemingly complicated Ψ instead of $\mathcal{Z}$ comes from the realization that Ψ obeys a simple differential equation. We will derive this equation in section V.B. Its solution for large L is dominated by a single eigenfunction of the differential operator. Armed with this knowledge, we will compute in section V.C quantities such as the average extension $\langle z \rangle$ and linking number $\langle Lk \rangle$ by substituting Ψ for $\mathcal{Z}$ in the thermodynamic relations (16).

V.B   The Schrödinger-Like Equation

The next step, then, is to determine the differential equation obeyed by $\Psi(\mathbf{g}, s; \mathbf{g}_i, 0)$ as a function of s. To do this,[51] consider the evolution over a short backbone segment of length ϵ:

$$\Psi(\mathbf{g}_f, s_f + \epsilon; \mathbf{g}_i, 0) = \int d\mathbf{g}_1 \left[\frac{1}{N}\int_{\substack{\mathbf{h}(s_f+\epsilon)=\mathbf{g}_f \\ \mathbf{h}(s_f)=\mathbf{g}_1}} [d\mathbf{h}(s)] \, \exp\left(-\frac{\delta E[\mathbf{h}(s)]}{k_B T}\right)\right] \Psi(\mathbf{g}_1, s_f; \mathbf{g}_i, 0). \qquad (18)$$

Here $\delta E[\mathbf{h}(s)]$ is the elastic energy of the short segment of rod from s_f to $s_f + \epsilon$. We introduced a normalizing factor N to get a continuum limit: as long as this factor does

not depend on $\tilde{f}$ or $\tilde{\tau}$ it will not enter the quantities of interest (see (16)). In this subsection we will compute the functional integral in (18), retaining terms up to first order in ϵ, and hence compute $d\Psi/ds_f$.

As $\epsilon \to 0$, we will see that only matrices g_1 close to g_f produce appreciable contributions to the path integral. It is therefore possible to write g_1 uniquely in the form $\mathsf{g}_1 = \exp(-T_\alpha \mathsf{L}_\alpha)\mathsf{g}_f$. Moreover, over the short segment under consideration we may take $\mathsf{h}(s)$ to interpolate between g_f and g_1 in the simplest way:

$$\mathsf{h}(s) = \exp\left(\frac{s - s_f - \epsilon}{\epsilon} T_\alpha \mathsf{L}_\alpha\right)\mathsf{g}_f. \tag{19}$$

The functional integral then reduces to an ordinary integral over $\vec{T}$:

$$\int d\mathsf{g}_1 \int_{\substack{\mathsf{h}(s_f+\epsilon)=\mathsf{g}_f \\ \mathsf{h}(s_f)=\mathsf{g}_1}} [d\mathsf{h}(s)] \to \int \exp\left(-\frac{|\vec{T}|^2}{12}\right) d^3\vec{T}. \tag{20}$$

We have suppressed an overall constant, absorbing it into N in (18). The exponential factor on the right side gives the invariant volume element of group space[52] near the point g_f. In the end, this factor will not modify the differential equation that we develop, but it is included here for completeness.

The energy functional $\delta E[\mathsf{h}(s)]$ can now be evaluated on the arclength slice of length ϵ. With the useful abbreviation

$$M_\alpha(\mathsf{g}_f) \equiv (\mathsf{g}_f \mathsf{L}_3 \mathsf{g}_f^{-1}, \mathsf{L}_\alpha) = (\sin\theta\sin\psi, -\sin\theta\cos\psi, \cos\theta), \tag{21}$$

we get that $\Omega_\alpha = -T_\alpha/\epsilon$ and $\hat{\Omega}_z = -\vec{M} \cdot \vec{T}/\epsilon$ which are constants (independent of s) over the short segment. Thus

$$\frac{\delta E[\mathsf{h}(s)]}{k_B T} = \frac{A}{2\epsilon}(T_1{}^2 + T_2{}^2) + \frac{C}{2\epsilon}T_3{}^2 + \tilde{\tau}\left(T_3 + \frac{T_1 M_1 + T_2 M_2}{1 + M_3}\right) - \epsilon\tilde{f}\cos\theta. \tag{22}$$

The factor $e^{-\delta E/k_B T}$ weights each path from $\mathsf{g}_1 = \exp(-\vec{T} \cdot \vec{L})\mathsf{g}_f$ to g_f; as $\epsilon \to 0$ it indeed kills all those g_1 which wander too far from g_f, i.e. all deformations where $T_\alpha \gtrsim \sqrt{\epsilon/A}$.

We also need to express $\Psi(\mathsf{g}_1)$ in terms of $\vec{T}$. Here and below we abbreviate $\Psi(\mathsf{g}_f, s_f, \mathsf{g}_i, 0)$ by $\Psi(\mathsf{g}_f)$. Define the left-acting (body-fixed) derivatives $\mathcal{J}_\alpha$ via

$$\mathcal{J}_\alpha \Psi(\mathsf{g}) \equiv [\mathsf{L}_\alpha \mathsf{g}]_{\beta i} \left.\frac{\partial \Psi}{\partial \mathsf{g}_{\beta i}}\right|_{\mathsf{g}}, \tag{23}$$

and similarly the right-acting (space-fixed) derivatives $\hat{\mathcal{J}}_i$. Then $\Psi(\mathsf{g}_1) = e^{-T_\alpha \mathcal{J}_\alpha}\Psi(\mathsf{g}_f)$ or

$$\Psi(\mathsf{g}_1) = \Psi - \vec{T} \cdot \vec{\mathcal{J}}\,\Psi + \frac{1}{2}T_\alpha T_\beta \mathcal{J}_\alpha \mathcal{J}_\beta \Psi + \cdots, \tag{24}$$

12

where we abbreviated still further by omitting the basepoint $\mathbf{g}_f$ on the right-hand side.

We can now combine (18,20,22,24) and perform the Gaussian integral $\mathrm{d}^3\vec{T}$. First complete the square, defining $\bar{T}_3 = \sqrt{C/2\epsilon}(T_3 + \epsilon\tilde{\tau}/C)$ and $\bar{T}_\alpha = \sqrt{A/2\epsilon}\,(T_\alpha + \epsilon\tilde{\tau}M_\alpha/A(1+\cos\theta))$, $\alpha = 1,2$. Choose the normalization N so that the limit $\epsilon \to 0$ reproduces Ψ. Collecting all order-ϵ terms and using $M_1{}^2 + M_2{}^2 = \sin^2\theta$ then gives

$$
\dot{\Psi} = \left\{ \frac{\tilde{\tau}^2}{2}\left(\frac{1}{C} + \frac{1}{A}\frac{1-\cos\theta}{1+\cos\theta}\right) + \tilde{f}\cos\theta + \frac{\tilde{\tau}}{A(1+\cos\theta)}(M_1\mathcal{J}_1 + M_2\mathcal{J}_2 + M_3\mathcal{J}_3 + \mathcal{J}_3) \right.
$$
$$
\left. + \tilde{\tau}\mathcal{J}_3\left(\frac{1}{C} - \frac{1}{A}\right) + \frac{1}{2}\left(\frac{1}{A}(\mathcal{J}_1{}^2 + \mathcal{J}_2{}^2) + \frac{1}{C}\mathcal{J}_3{}^2\right) \right\}\Psi. \tag{25}
$$

Further consolidation then gives $\dot{\Psi} = -\left(\mathcal{H} + \mathcal{E}_0\right)\Psi$, where

$$
\mathcal{E}_0 \equiv -\left(\tilde{f} + \frac{\tilde{\tau}^2}{2C}\right) \tag{26}
$$

and the differential operator $\mathcal{H}$ is defined by

$$
\mathcal{H} = \frac{K}{A}\left[-\frac{1}{2K}\vec{\mathcal{J}}^2 + K(1-\cos\theta) - \frac{\tilde{\tau}^2}{4K}\frac{(1-\cos\theta)^2}{1+\cos\theta} - \frac{1}{2K}\left(\frac{A}{C}-1\right)\mathcal{J}_3{}^2 \right.
$$
$$
\left. - \frac{\tilde{\tau}}{K}\left[\left(\frac{A}{C}-\frac{1}{2}\right)\mathcal{J}_3 + \frac{1}{2}\hat{\mathcal{J}}_z\right] - \frac{\tilde{\tau}}{4K}\frac{1-\cos\theta}{1+\cos\theta}(\mathcal{J}_3 + \hat{\mathcal{J}}_z) \right]. \tag{27}
$$

We have arranged the terms in (27) to facilitate a systematic expansion in powers of K^{-1}, where $K \equiv \sqrt{A\tilde{f} - \tilde{\tau}^2/4}$.

An important property of $\mathcal{H}$ is that it commutes with both the operators $\mathcal{J}_3$ and $\hat{\mathcal{J}}_z$. The physical meaning of this property is simply that a uniform rotation of the rod about the constant axis $\hat{e}_z$ changes nothing, and (by the rod's isotropy) neither does uniform rotation of the rod about its own $\hat{t}$-axis.

Thus the unnormalized propagator Ψ obeys a differential equation which is of Schrödinger type, in imaginary time. The derivatives $\mathcal{J}_\alpha$ correspond to $i/\hbar$ times the usual angular momentum operators, and so on. In the next section, we will exploit the quantum mechanical analogy to find solutions to this equation which will in turn allow us to determine the quantities $\langle z \rangle$ and $\langle Lk \rangle$.

V.C   Solution and Results

It is now possible to make a direct connection between the eigenvalue problem associated to (27) and our polymer problem.

In ordinary quantum mechanics, the solution to the Schrödinger equation for a symmetric top can be written as a superposition of Wigner functions:[53]

$$\Psi(\mathbf{g}, t) = \sum_{jmk} c_{jmk} \mathrm{e}^{-\mathrm{i}\mathcal{E}_{jmk}t} \, \mathcal{D}^j_{mk}(\mathbf{g}).\tag{28}$$

Here m and k are angular momenta associated with the operators $\mathcal{J}_3$ and $\hat{\mathcal{J}}_z$, and $\mathcal{E}_{jmk}$ is the eigenvalue associated with the Wigner function $\mathcal{D}^j_{mk}$. The coefficients c_{jmk} characterize the initial state at time $t = 0$.

It may seem difficult to apply (28) to our statistical problem, since in our case $\mathcal{J}_3$ and $\hat{\mathcal{J}}_z$ are real, antisymmetric operators with no basis of real eigenvectors. Similarly, and unlike the case of the wormlike chain, $\mathcal{H}$ has no particular symmetry. A little thought shows, however, that these are surmountable problems. Since one end of our rod is clamped, the initial probability distribution $\Psi(\mathbf{g}, 0)$ may be taken to be a delta-function concentrated on $\mathbf{g} = 1$, the identity matrix $\theta = \psi + \phi = 0$. This Ψ is indeed an eigenstate of $\mathcal{J}_3 - \hat{\mathcal{J}}_z$ with eigenvalue $m - n = 0$. The other end of the rod may also be considered clamped to $\theta = 0$, but since we work in the fixed-torque ensemble the overall rotation $\psi + \phi$ is free to take any value. In other words, after evolving $\Psi(\mathbf{g}, 0)$ to $\Psi(\mathbf{g}, L) = \mathrm{e}^{-(\mathcal{E}_0 + \mathcal{H})}\Psi(\mathbf{g}, 0)$ we need to *project* it to the eigenspace with $\mathcal{J}_3 + \hat{\mathcal{J}}_z = 0$. Since as noted earlier $\mathcal{J}_3$ and $\hat{\mathcal{J}}_z$ both commute with $\mathcal{H}$, we may perform the projection on $\Psi(\mathbf{g}, 0)$ instead.

Thus for our problem we should simplify (27) by setting $\mathcal{J}_3 = 0$ and $\hat{\mathcal{J}}_z = 0$, obtaining the differential equation that appeared in earlier work:[20, 19] $\dot{\Psi} = -(\mathcal{H} + \mathcal{E}_0)\Psi$, where

$$\mathcal{H} = \frac{K}{A}\left[-\frac{\vec{\mathcal{J}}^2}{2K} + \left(K - \frac{\tilde{\tau}^2}{4K}\frac{1 - \cos\theta}{1 + \cos\theta}\right)(1 - \cos\theta)\right],\tag{29}$$

$$K \equiv \sqrt{A\tilde{f} - \tilde{\tau}^2/4},\tag{30}$$

and $\mathcal{E}_0 = -(\tilde{f} + \tilde{\tau}^2/2C)$. The major difference between this equation and that obtained for ordinary (non-twist storing) polymers is that the long-wavelength cutoff is now controlled by K instead of $\sqrt{A\tilde{f}}$.

The operator in (29) really is symmetric, and hence will have real eigenvectors (modulo a subtlety discussed in appendix B). The solutions to our Schrödinger-like equation will then have the form (28) with it replaced by arclength s. For a sufficiently long chain, the lowest "energy" solution will then dominate Ψ. The thermodynamic properties of the polymer can then be determined by remembering that Ψ, the unnormalized propagator, becomes equal to a constant times the partition function $\mathcal{Z}$, and applying (16).

We gain further confidence in the above analysis when we note that the terms set to zero in (27) include some which are linear in the applied torque τ. For reasons outlined in section III, we do not expect these terms to play a role in the determination of the lowest energy eigenvalue. The model that we defined is non-chiral and therefore cannot tell the difference between over- and undertwisting.

We must now compute the lowest eigenvalue of the differential operator in (29). Finding it would be a straightforward task were it not for the singularity in the potential term when $\theta \to \pi$. This singularity is associated with the backbone tangent $\hat{t}$ looping around to point anti-parallel to the end-to-end displacement vector $+\hat{e}_z$. Physically, this situation corresponds to the onset of supercoiling. When the applied torque is too high or the tension is too low, the chain will begin to loop over itself. Since real chains cannot pass through themselves, they begin to form plectonemes. In our *phantom chain* model, there is no self-avoidance, and so the chains can pass through themselves, shedding a unit of Lk as they do. The mathematical pathology associated with the $\theta \to \pi$ singularity in (29) is therefore an inevitable consequence of our model's neglect of self-avoidance.

The physical breakdown of the *phantom chain* model and the corresponding mathematical problem of the $\theta \to \pi$ singularity can be avoided by assuming that the backbone tangent $\hat{t}$ remains nearly parallel to the $+\hat{e}_z$-axis. Such a situation is indeed realistic for a chain under sufficient tension, or more precisely, for a sufficiently large K (30). In this regime, we can then perform a perturbative expansion about $\theta = 0$. The singularity of (29) does not affect low orders of perturbation theory. The singularity can still enter nonperturbatively via "tunneling" processes, in which the straight $\theta \approx 0$ configuration hops over the potential barrier in (29), but these will be exponentially suppressed if the barrier is sufficiently high, a condition made more precise in appendix B. The perturbative regime is experimentally accessible: we will argue that it corresponds to the solid symbols on Figure 1. Outside this regime, the *phantom chain* model is physically inappropriate, as explained above, and so a full nonperturbative solution of our model would not be meaningful.

We can simplify the problem by changing variables from θ to $\rho^2 \equiv 2(1 - \cos\theta)$. In terms of ρ the spherical Laplacian $\mathcal{J}^2 = \frac{1}{\sin\theta}\frac{\partial}{\partial\theta}\sin\theta\frac{\partial}{\partial\theta}$ becomes $(1 - \rho^2/4)\partial_\rho{}^2 + (1 - 3\rho^3/4)\rho^{-1}\partial_\rho$, so

$$\mathcal{H} = \frac{K}{A}\left[-\frac{\nabla^2}{2K} + \frac{K}{2}\rho^2 + \frac{1}{2K}\left(\frac{3\rho}{4}\frac{\partial}{\partial\rho} + \frac{\rho^2}{4}\frac{\partial^2}{\partial\rho^2} - \frac{\tilde{\tau}^2\rho^4}{16 - 4\rho^2} \right) \right] \qquad (31)$$

where $\nabla^2 = \rho^{-1}\partial_\rho\rho\partial_\rho$. We have not made any approximation yet.

We now construct a perturbative solution to the eigenvalue problem defined by (31). In the quantum mechanical analogy this equation describes a two-dimensional

anharmonic oscillator, with ρ interpreted as a radial coordinate; thus the problem can be solved using the method of raising and lowering operators.

Switching to Cartesian coordinates, we set

$$\mathcal{A}_\pm = \sqrt{\frac{K}{2}} \left(x \mp \frac{1}{K} \frac{\partial}{\partial x} \right), \qquad \text{and} \qquad \mathcal{B}_\pm = \sqrt{\frac{K}{2}} \left(y \mp \frac{1}{K} \frac{\partial}{\partial y} \right). \qquad (32)$$

Now (31) can be rewritten as $\mathcal{H} = \mathcal{H}_0 + \delta\mathcal{H}$, where

$$\mathcal{H}_0 = \frac{K}{A} \left(\mathcal{N}_a + \mathcal{N}_b + 1 \right), \qquad \text{and}$$

$$\delta\mathcal{H} = \frac{K}{A} \left[-\frac{1}{8K} \left(1 - \frac{1}{4} \left\{ (\mathcal{A}_+^2 - \mathcal{A}_-^2) + (\mathcal{B}_+^2 - \mathcal{B}_-^2) \right\}^2 \right) + \mathcal{O}(K^{-3}) \right]. \qquad (33)$$

Here $\mathcal{N}_a \equiv \mathcal{A}_+ \mathcal{A}_-$ and $\mathcal{N}_b \equiv \mathcal{B}_+ \mathcal{B}_-$ correspond to the usual occupation number operators in the quantum mechanical analogy. It is now straightforward to calculate the lowest energy eigenvalue as an expansion in K^{-1} to obtain[19]

$$\mathcal{E} = \mathcal{E}_0 + \frac{K}{A} \left(1 - \frac{1}{4K} - \frac{1}{64K^2} + \cdots \right). \qquad (34)$$

Remarkably, this is exactly the same formula as the one appearing in the wormlike chain model; the only difference is that K is now defined by (30) instead of by $\sqrt{A\tilde{f}}$. The last two terms retained will now give anharmonic corrections to the simple lowest-order calculation announced earlier.[18] The ellipsis represents terms of higher order in K^{-1} than the ones kept. We explore the status of such terms in appendix B. In particular, the last term of (31) has been dropped altogether. Since the expectation value of this term is obviously divergent at $\rho = 4$ (*i.e.* the antipode $\hat{t} = -\hat{z}$), a certain amount of justification will be needed for dropping it.

From this eigenvalue, the mean extension and the average linking number for a given tension and torque can be found using (16), (28), and (34):

$$\left\langle \frac{z}{L} \right\rangle = 1 - \frac{1}{2K} \left(1 + \frac{1}{64K^2} + \mathcal{O}(K^{-3}) \right), \qquad \text{and} \qquad (35)$$

$$\left\langle \frac{Lk}{L} \right\rangle = \frac{\tilde{\tau}}{2\pi} \left(\frac{1}{C} + \frac{1}{4AK} + \mathcal{O}(K^{-3}) \right). \qquad (36)$$

More accurate versions of these formulæ are given in appendix B. By solving the second of these equations for the torque we obtain the new, effective twist rigidity C_{eff} by noting that $\tilde{\tau}(\tilde{f}, Lk) \approx (2\pi Lk/L) C_{\text{eff}}(\tilde{f}) + \mathcal{O}(K^{-3})$, where $C_{\text{eff}}(\tilde{f})$ is given by the formula (8). This formula describes the "thermal softening" of the twist rigidity alluded to earlier. The effective rigidity $C_{\text{eff}}(f)$ is reduced from the bare, microscopic value by a factor which arises from thermal fluctuations.

16

Combining (35) and (36) together with the definition of K in (30) produces a formula for the average end-to-end extension for a polymer subject to a linking number constraint and an applied tension. In section VI we will compare this theoretical prediction to the experimental results of Strick *et al.*[14] and Allemand and Croquette.[16]

V.D   Onset of Non-Perturbative Corrections

The theory described above is only valid in the regime where the *phantom chain* model is appropriate. In this section, we extend our analysis by *estimating* the effect of plectoneme formation close to its onset. As discussed above, our model is unable to include such effects quantitatively, as it lacks the self-avoidance interaction which stabilizes plectonemes. Instead, in this section we will suppose that the main consequence of the singularity is to allow each segment of the polymer to be in one of two configurations. In the first instance, the polymer fluctuates about a nearly straight conformation and can therefore be described by the theory developed in the preceding sections. In the second instance, the polymer is driven across the "tunneling" barrier into a standard kink conformation as depicted in Figure 2, gaining approximately one unit of Writhe. Our improved formulæ will have *no new fitting parameters* beyond the ones already introduced.

We are interested only in the initial stages of plectoneme formation and so it will be sufficient to approximate each plectonemic coil by a circle. The energy required to form such a loop is

$$\frac{\Delta E}{k_{\mathrm{B}}T} = \frac{A}{2}\frac{2\pi R}{R^2} + \tilde{f}2\pi R - 2\pi|\tilde{\tau}|. \tag{37}$$

Here the first two terms represent the energy costs associated with bending the polymer and contracting against the imposed tension. The last term gives the elastic twist energy released as Twist gives way to Writhe. Maximizing the energy release, we find the optimal radius of a coiled segment to be $R = \sqrt{A/2\tilde{f}}$, so that for $\tilde{\tau} > 0$ the presence of a kink lowers the energy of the polymer by $\Delta E_-/k_{\mathrm{B}}T = 2\pi(\sqrt{2A\tilde{f}} - \tilde{\tau})$.

We now imagine the polymer to be made up of segments of length $2\pi R$. Each of these segments may be in the extended or the plectonemic kink configuration. Actually, we will consider two possible types of kink: one in which a unit of Twist is shifted into Writhe, and its mirror image which generates a negative Writhe as well as a counteracting positive Twist. The reverse kinks are energetically unfavorable for appreciable applied torque, but we retain them to eliminate any asymmetry in the excess linking number.

For the modest applied torque considered here, it will be sufficient to treat a dilute gas of positive and negative kinks. Denoting the population of kinks by n_- and that of

17

reverse kinks by n_+, we have

$$\langle n_\pm \rangle = \frac{\kappa L}{2\pi R} \exp\left(-\frac{\Delta E_\pm}{k_\mathrm{B} T}\right). \tag{38}$$

Here $\Delta E_+ = 2\pi(\sqrt{2A\tilde{f}} + \tilde{\tau})$ is the energy of a reverse kink, and κ is a numerical factor of order unity arising ultimately from a functional determinant. Since we do not know how to compute κ we set it equal to unity.

The effect of the kink/anti-kink gas is to modify (35) and (36), producing shifts in the average extension and average linking number:

$$\Delta\left\langle \frac{z}{L} \right\rangle = -\left(e^{-\Delta E_-/k_\mathrm{B} T} + e^{-\Delta E_+/k_\mathrm{B} T} \right) \tag{39}$$

$$\Delta\left\langle \frac{Lk}{L} \right\rangle = \frac{1}{2\pi} \sqrt{\frac{2\tilde{f}}{A}} \left(e^{-\Delta E_-/k_\mathrm{B} T} - e^{-\Delta E_+/k_\mathrm{B} T} \right). \tag{40}$$

These expressions are to be added to (35) and (36). The latter expression can then be solved for $\tilde{\tau}$ to get a corrected version of (8).

The model proposed here for plectoneme formation is too simplified to give quantitative predictions about the non-perturbative regime. However, the model does allow us to predict the onset of these effects and confirm that the data we select are not affected by plectoneme formation (see Figure 1).

VI Fit Strategy and Results

The extension function $\langle z(f, Lk) \rangle$ derived in the previous sections describes an achiral elastic rod. Before making direct comparisons of this formula to experimental data, we will extend the model somewhat. So far we have neglected structural changes in the DNA at a microscopic level. In particular, we have omitted effects related to the intrinsic stretching along the polymer backbone. Recent experiments have investigated these effects;[10, 54] in particular, Wang et al. found a small change in the relative extension of f/γ, where $\gamma = 1100$ pN is the intrinsic stretch modulus. For moderate forces we may simply add this shift to the extension formula found in the previous section.[55, 12] For the highest forces we consider (8.0 pN), this translates into a relative extension of about 0.007, which is hardly noticeable in Figure 1. Nevertheless, we will include this correction as it improves the quality of our fit slightly without introducing a new fitting parameter.

In addition, we will also consider the possibility of elastic couplings which do not respect the inversion symmetry of the model that we consider. In reality the DNA we

seek to describe is chiral, and so at some level we expect this fact to show up as an asymmetry between overtwisting and undertwisting in Figure 1. One way that chirality might enter a model for DNA is through an intrinsic twist-stretch coupling.[22, 42, 43] This coupling results in a change in relative extension of $-k_{\mathrm{B}}TD\omega_0^2\sigma/\gamma$, where D is the twist-stretch coefficient. The near symmetry in the data of Figure 1 indicates that the effects of such a coupling will be small in the region of interest. Although the coefficient D will turn out to be comparable in size to the bending coefficient A, the shortening due to bend fluctuations dominates that due to the elastic twist-stretch coupling. This disparity arises because bend fluctuations are diverging as $K \to 0$.

As mentioned in section III, an anisotropy between the "tilt" and "roll" elastic constants coupled together with the associated twist-bend coupling term might also produce an asymmetry between positive and negative σ. We investigate this possibility in appendix A and find that the corresponding *chiral entropic elasticity* terms are not measurably different from the twist-stretch model over the range of stretching forces studied.

Putting the intrinsic corrections associated with γ and D together with the perturbation theory result of the last section, we obtain a theoretical prediction for the relative extension as a function of applied force and overtwisting. For the purposes of comparison to experiment, we will now switch from the variable Lk to the relative overtwist σ which is defined with respect to the helical pitch of DNA: $\sigma = 2\pi Lk/\omega_0 L$. Then,

$$\left\langle \frac{z(f,\sigma)}{L} \right\rangle = 1 - \left(2\sqrt{\frac{Af}{k_{\mathrm{B}}T} - \frac{\tilde{\tau}^2}{4} - \frac{1}{32}} \right)^{-1} + \Delta\left\langle \frac{z}{L} \right\rangle + \frac{f - k_{\mathrm{B}}TD\omega_0^2\sigma}{\gamma} + \frac{A}{K^2 L}. \quad (41)$$

Formula (41) is our final result for the high-force (or more precisely, large K) extension of a twist-storing polymer subject to a torsional constraint. Here $\Delta\langle z/L \rangle$ is the expression in (39). To compare our result to the experimental data,[14, 16] we solved (30), (36), and (40) for $\tilde{\tau}$ in terms of $\tilde{f}, \sigma$, then substituted $\tilde{\tau}$ and K into (41).

Apart from the intrinsic stretch and twist-stretch terms described above, (41) contains two additional small refinements. One of these appears in the last term, where finite-size effects have been accounted for. This term can be understood by writing the extension as an expansion in terms of the transverse components of the backbone tangent. Defining the complex variable $\alpha(s) = \hat{t}(s) \cdot (\hat{e}_{\mathrm{x}} + i\hat{e}_{\mathrm{y}})$ and its Fourier components α_p, we have to lowest order

$$\left\langle \frac{z}{L} \right\rangle = 1 - \frac{1}{2}\sum_p \langle |\alpha_p|^2 \rangle + \cdots . \quad (42)$$

The leading entropic reduction of $\langle z \rangle$ in (35) is then easy to evaluate, including finite-length effects. As the main effect of an applied torque is to decrease the effective force and change the low wavenumber cutoff in our theory from $\sqrt{A\tilde{f}}$ to K, we know how to modify the usual tangent-tangent correlation function to yield

$$\sum_p \langle |\alpha_p|^2 \rangle = \frac{4A}{L} \sum_{n=1}^{\infty} \frac{1}{A^2 \left(\frac{2\pi n}{L}\right)^2 + K^2}$$
$$= \frac{1}{K}\left(1 - \frac{2A}{KL}\right). \tag{43}$$

This expression should be compared with the leading-order correction obtained from the infinite-rod calculation in section V:

$$\sum_p \langle |\alpha_p|^2 \rangle \approx \frac{2A}{\pi} \int_0^{\infty} \frac{1}{(Aq)^2 + K^2}\mathrm{d}q$$
$$\approx \frac{1}{K}. \tag{44}$$

The difference between the two terms is $2A/LK^2$. To obtain the finite length formula we must subtract this difference from the result obtained in the last section; the resulting correction appears in the last term of (41). Note that for the restricted values of K that we consider (see below), this contribution to z/L never exceeds 0.002 for the data set we analyze.

The other refinement introduced in (41) is that for convenience we replaced $(1/2K)(1 + 1/64K^2)$ by $(K^2 - 1/32)^{-1/2}$. Since we will restrict our fit to $K^2 > 3$, the difference between these expressions is negligible. Finally, in Appendix B we give even more elaborate versions of (36) and (41), in which higher-order terms of perturbation theory have been retained; these corrections are small though not negligible at low forces.

We have now established an expression for the mean extension as a function of applied tension and torque. Using the ENS group's data,[14, 16] we fit this formula (actually, the more accurate one given in appendix B) to determine the parameters in our model: the microscopic bend persistence length A, twist persistence length C, twist-stretch coupling D, and polymer arclength L. Of these parameters, only C and D are really unknown; A has already been measured in other experiments, and L can be determined from the points with $\sigma = 0$ using the ordinary worm-like chain model. The agreement between our best fit value of A and earlier experiments[10, 7, 26] serves as a check on the theory. Other parameters appearing in (41), namely $\omega_0 = 1.85\,\mathrm{nm}^{-1}$ and $\gamma = 1100\,\mathrm{pN}$,[10] are independently known and are not fit.

The least squares fit was performed using a gradient descent algorithm[56] in the parameter space defined by A, C, D, and L. The best fit was obtained for $A = 49\,\mathrm{nm}$,

$C = 109$ nm, $D = 67$ nm, and $L = 15.6\mu$m. Here L is the length of the construct from Allemand and Croquette's experiment.[16] The corresponding length for the Strick *et al.* data set[14] was determined separately using the $\sigma = 0$ points from that set and was not fit. In all, 69 data points from the experiments of Strick *et al.*[14] and of Allemand and Croquette[16] were used in the procedure. The data points were selected based on three criteria. The first cuts were made on physical grounds. It is known that for high applied forces ($f > 0.4$ pN) DNA undergoes structural transformation or strand separation when $\sigma < -0.01$ or $\sigma > 0.03$ (D. Bensimon, private communication); here of course we cannot use linear elasticity theory. We therefore omitted such points from the right side of Figure 1. (No points were omitted from the left side.) To avoid biasing the data, in the fit we excluded the *symmetric* region $|\sigma| > 0.01$ from the set of points used with $f > 0.4$ pN.

The second set of cuts was applied for mathematical reasons. Our perturbative expansion is in powers of K^{-1}: we required $K^2 > 3$. We discuss this choice in appendix B; for now we note that perturbation theory produces excellent agreement with experiment for the wormlike chain[12] even for $K > 1$. Choosing $K^2 > 3$ eliminates all of the $f = 0.1$ and 0.2 pN data points from our fit. To confirm that we were being selective enough, we tried other values of the threshold (between 2.5 and 4.5). This action did not significantly alter our fit results: in every case we found $C > 100$ nm.

Finally, in addition to these two sets of data cuts, we also imposed a "tunneling" criterion described in appendix B: the idea is to ensure that the lowest energy eigenvalue of the operator $\mathcal{H}_0$ in (33) is smaller than the barrier that restrains the system from falling into the unphysical singularity.

The reasonable agreement in Figure 1 between our theoretical curves and the data *outside the region we fit* (including the 0.1 and 0.2 pN curves) indicates that our choice of cuts is a conservative one. As a further check, the dashed lines in Figure 1 show our fitting function without the non-perturbative correction described in section V.D: we see that these lines do not deviate from the solid lines in the range of data we retained.

VII Discussion

The global fit shown in Figure 1 indeed resembles the experimental data. The least squares fit determined the bending stiffness, the twist rigidity and the intrinsic twist-stretch coefficient of DNA. As stated earlier, the fit to the bending rigidity produced the known value and thus serves as a check on the theory. The chiral asymmetry is a small effect, and so the available data do not afford a precise determination of the twist-stretch

coupling D. Thus our fit is mainly a measurement of C.

The twist rigidity obtained by the fitting procedure is somewhat higher than what earlier experiments have found (see section III). We cannot give a quantitative estimate of our fit parameter errors, since some of the data[14] do not have error bars, but we note that forcing $C = 85$ nm or less gives a visibly bad fit. One might worry that this discrepancy was due to some sort of failure of perturbation theory, despite our great care on this point. The fact that we keep finding large C as we tighten the data cuts gives us additional confidence on this point. Similarly, our large value is not an artifact of DNA denaturation induced by tension, since that would lead to a spuriously *low* fit value. There remains the intriguing possibility that on the contrary, imposed tension *suppresses* spontaneous local denaturation, increasing the integrity of the DNA duplex (J. M. Schurr, private communication); in this case our large C more accurately reflects the linear elasticity than the other, lower, values.

The discrepancy with earlier work may be more apparent than real, however: if we do not allow for a tension-dependent thermal reduction of the twist rigidity as in (8) and instead fit the data to a constant twist rigidity, then we obtain $C_{\text{eff}} = 82$ nm, a value closer to those found in the other experiments.[36] The quality of this fit, obtained with a tension-independent rigidity, is slightly poorer. In any case, a large value of C/A is not paradoxical and in particular need not imply a negative Poisson ratio for our model's rod: random natural bends in DNA reduce the effective bend stiffness A measured in stretching experiments, but not C,[50] and so the ratio of C to the true elastic bend stiffness is closer to unity than it appears from our effective-homopolymer model.

Recently, Bouchiat and Mézard[20] have also determined the twist rigidity of DNA using the experimental results of Strick *et al.*[14] They derived formulæ equivalent to (35) and (36). Then using an exact ground state solution to a cut-off version of (31), they reproduced the observed extension curve $\langle z(f, \sigma) \rangle$ in Figure 1a over a wider range than we have shown. The result of this calculation is a ratio of C/A of approximately 1.7.

While both approaches are similar, our perturbative approach precludes us from analyzing the lowest force curves that Bouchiat and Mézard discussed. As described above, we excluded these data because we expect physical difficulties with the *phantom chain* model in this regime; the same difficulties, it would seem, apply to the analytical results of Bouchiat and Mézard. In particular, at small applied tension, the backbone's tangent vector $\hat{t}$ will wander from the z-axis. If it wanders too far, the system will be able to see through the tunneling barrier to the singularity; or in other words, the results will be corrupted by the failure of Fuller's formula for *Wr*. Bouchiat and Mézard approached this problem by introducing a new intermediate-length cutoff $b = 6$ nm into the problem.

The physical meaning of this cutoff in terms of the mechanical properties of DNA is not clear to us. Moreover, taking it to be 2.5 nm or less spoiled the simultaneous fit at all values of f.

In contrast, our perturbative treatment avoids the singular-potential problem altogether by restricting to a regime where the *phantom chain* model is valid. Our model has no extra scale corresponding to b, and yet fits all fixed-force curves in its domain, in two different experiments, with one value of C.

In their paper, Bouchiat and Mézard also gave Monte Carlo results. Earlier work by Marko and Vologodskii has also taken this approach.[21] Here it is possible to implement self-avoidance, though knot rejection is still difficult. The advantage of analytic formulæ such as (41) is that they permit global, systematic least-squares fitting of $\langle z(f, \sigma) \rangle$ to the data. Moreover, for practical reasons Monte Carlo simulations must again impose a short-distance cutoff of at least several times the DNA radius, unlike our analytical approach.

VIII   Conclusion

In this paper we have investigated the statistical mechanics of a twist-storing polymer. This type of molecule differs from a traditional polymer in being unable to relax out an applied excess Link. When such a chain is left unconstrained, the twist simply decouples from the bend fluctuations. The thermally accessible conformations are then identical to those for an ordinary polymer. In the case that such a polymer is subject to a torsional constraint, however, there will be a coupling between the bend fluctuations and the twist. It is this coupling that we have investigated. One of our goals was to show how single-molecule stretching experiments can provide a new window onto the nanometer-scale mechanical properties of DNA.

Due to the complications associated with self-avoidance, we considered only chains held nearly straight by tension, then analyzed the statistical mechanics of the resulting "torsional directed walk". We mapped the polymer partition function onto the solution of a Schrödinger-type equation for the orientation distribution function. From this solution, we were able to find the entropic extension and the overtwisting of a polymer subject to a tension f and relative Link excess σ.

The theory we developed quantitatively reproduces the results of supercoiled single-molecule DNA stretching experiments[14, 16] (see Figure 1). The agreement was achieved by fitting the twist persistence length, yielding $C = 109$ nm. The large twist rigidity differentiates DNA from traditional polymers and makes possible the coupling of the

twist and bend degrees of freedom that plays a central role in our theory.

Apart from reproducing the experimentally observed physics, our formulæ make another prediction: the twist rigidity is renormalized (see (36)). The effective rigidity $C_{\text{eff}}(f)$ is a function of the applied tension. According to (8), it is hardest to twist the polymer when it is pulled straight; this is the bare, microscopic stiffness. It is the same rigidity that resists twist at the shortest length scales, and so enters the energetics of structures such as the nucleosome. As the tension is relaxed, thermal fluctuations begin to play a role. Now when a torque is applied, the polymer does not resist as much; the bend fluctuations have softened the torsional rigidity by absorbing some of the imposed excess Link. As discussed above, this phenomenon is purely thermal; no such effect appears in the linear elasticity of a macroscopic beam for small applied torque.

If one naïvely extends this thermal effect to zero tension, one sees that the torsional rigidity vanishes completely. Of course, our *phantom chain* model precludes us from considering this case; however, other recent work[57] has considered this related problem using an explicit self-avoidance term: indeed the effects of a torsional rigidity do become unimportant to the behavior of twist-storing polymers at zero applied tension or, equivalently, at extremely long length scales.

Appendix A: Chiral entropic elasticity

In this appendix we introduce an additional element of realism into our model, namely the intrinsic helical pitch $2\pi/\omega_0$. For DNA this pitch corresponds to $\omega_0 = 1.85/\text{nm}$. The helical structure breaks the inversion symmetry of the problem by allowing two additional terms in the energy functional.[27] In principle these explicitly chiral terms could introduce an asymmetry between overtwist and undertwist into our results. We will find this *chiral entropic elasticity* and show that it has a different dependence on stretching force from the intrinsic twist-stretch effect discussed in section VI. Thus in principle the two effects could be distinguished experimentally.

In this appendix we are interested in chiral effects, manifested by odd powers of σ in the extension $z(f, \sigma)$, in a model of DNA without intrinsic stretching. We will see that such terms are small. Hence we can use a simpler calculation than the one in the main text: we will drop $\mathcal{O}(\sigma^2)$ and higher, and we will use the Gaussian (or equipartition) approximation to the statistical sums. Since odd-power terms are completely absent in the achiral model of section V above, we can simply add the ones we find to the results of that model to get a leading approximation to the full *chiral entropic elasticity* formula.

Another approximation we will make will be to drop terms suppressed by powers of

$1/\omega_0$, since this length scale is much shorter than both the persistence lengths and the scale $\sqrt{A/\tilde{f}}$ of important fluctuations.

As discussed in section III, chirality can enter through the anisotropic bending rigidities associated with the "roll" and "tilt" axes of DNA monomers. In this appendix we will choose a material frame different from the one in the main text: here our frame rotates with the intrinsic helical twist. This choice is convenient in that the anisotropic elasticity appears constant in this frame: (1) becomes simply

$$\frac{E_{\text{bend}}}{k_{\text{B}}T} = \frac{1}{2} \int_0^L \mathrm{d}s \left(A_1' \Omega_1{}^2 + A_2' \Omega_2{}^2 \right), \qquad \text{and} \qquad \frac{E_{\text{twist}}}{k_{\text{B}}T} = \frac{1}{2} \int_0^L C' \Omega_3{}^2 \, \mathrm{d}s. \qquad (45)$$

Here we have introduced *two* microscopic bending constants, A_1' and A_2'. Now even the unstressed state will be chiral: as the body-fixed frame $\{\hat{E}_1, \hat{E}_2, \hat{E}_3 = \hat{t}\}$ rotates uniformly at frequency ω_0 along the polymer, it turns the bend anisotropy with it. Since the $\hat{E}_1$-axis corresponds to the short axis of a basepair, we expect $A_1' > A_2'$.

Apart from the bending anisotropy, the symmetries of DNA admit an explicitly chiral term associated to a twist-bend coupling with coefficient G.[27] With these two terms, the mechanical-equilibrium state of the stressed molecule will no longer be given by the uniformly twisted configuration. Instead, we make an *ansatz* for a new helical ground state: $\mathbf{g}_0 = \exp(\zeta \mathsf{L}_1) \exp(\omega s \mathsf{L}_3)$, to be justified below. Here ω includes a finite piece associated with the rotation of the unstressed molecule, so that $\omega = \omega_0(1 + \sigma)$. The small angle ζ remains to be determined by the condition of mechanical equilibrium. The elastic energy functional for the model is then given by:

$$\frac{E}{k_{\text{B}}T} = \frac{1}{2} \int_0^L \mathrm{d}s \left\{ A_1' \Omega_1{}^2 + A_2' \Omega_2{}^2 + C'(\Omega_3 - \omega_0)^2 + 2G\Omega_2(\Omega_3 - \omega_0) \right\} - \tilde{f} \cdot z. \qquad (46)$$

In contrast to the discussion in the main text, in this appendix we will work in the fixed-Lk ensemble. Thus we do not need any Lagrange multiplier associated with the Link constraint.

It will prove convenient to introduce the combinations $\bar{A} = (A_1' + A_2')/2$ and $\hat{A} = (A_1' - A_2')/2$. We emphasize that $\bar{A}$ is not necessarily equal to A from the coarse-grained model (1); the exact relationship will emerge in due course below. The chiral terms that couple to the intrinsic helical frequency ω_0 are then proportional to $\hat{A}$ and G. Note that $\hat{A} > 0$.

We can now determine the helix angle ζ characterizing the mechanical-equilibrium state. First write a small fluctuation from $\mathbf{g}_0$ as $\mathbf{g}(s) = \tilde{\mathbf{g}}(s)\mathbf{g}_0(s)$ with $\mathbf{g}_0$ as above and $\tilde{\mathbf{g}}(s) \equiv \mathrm{e}^{-T_\alpha(s)\mathsf{L}_\alpha}$. Substituting into (11,12) then yields the Ω_i's. Setting the first variation of (46) to zero then yields three equations expressing the condition that $\mathbf{g}_0$ be the stressed

mechanical-equilibrium state. One of these selects ζ:

$$\zeta = -\frac{G\sigma}{A_2' + \tilde{f}/{\omega_0}^2} \approx -\frac{G\sigma}{A_2'}. \tag{47}$$

The other two are satisfied trivially, justifying our *ansatz* for $\mathbf{g}_0$. In deriving the above relations we used the fact that we are working in the fixed-σ ensemble. Thus the boundary conditions clamp the rod at both ends, fixing $\vec{T} = 0$ there, and so we may discard total derivative terms.

For illustration, and to keep the calculation simple, we will now make the additional assumption that the chiral parameters $\hat{A}, G$ are both smaller than $\bar{A}, C$, and accordingly work to leading nontrivial order in the former. We can then easily diagonalize the part of the energy involving the latter using Fourier modes. Setting $(T_1(s)+\mathrm{i}T_2(s))\mathrm{e}^{\mathrm{i}\omega s} \equiv \sum \mathrm{e}^{\mathrm{i}qs}\alpha_q$ and $T_3(s) \equiv \sum \mathrm{e}^{\mathrm{i}qs}\phi_q$ (note that $\phi_{-q} = \phi_q^*$) yields

$$\frac{E}{k_{\mathrm{B}}T} = -\tilde{f} \cdot L + \xi_0 + \xi_1 + \xi_2, \tag{48}$$

where

$$
\begin{aligned}
\xi_0 &= \frac{L}{2}\sum_p \left[\left(\bar{A}p^2 - \omega(C'\sigma + 2G\zeta)p + \tilde{f}\right)|\alpha_p|^2 + C'p^2|\phi_p|^2\right] \\
\xi_1 &= \frac{\mathrm{i}L}{2}\sum_p \left[G(\omega - p)p + \zeta\left(A_1'\omega(\omega - p) + \tilde{f} - C'\omega p\right)\right](\phi_p\alpha_{\omega-p} - \text{c.c.}) \\
\xi_2 &= \frac{L}{2}\sum_p \left[\frac{\hat{A}}{2}p(p - 2\omega) - \frac{G\omega\zeta}{2}p\right](\alpha_p\alpha_{2\omega-p} + \text{c.c.}).
\end{aligned}
\tag{49}
$$

In the above formulæ, $\omega \equiv \omega_0(1+\sigma)$ gives the angular frequency for the stressed minimal-energy state. The sums are for $-\infty < p < \infty$ (the physical short-scale cutoff will prove immaterial). As mentioned above, we will treat $\xi_{1,2}$ as perturbations to ξ_0.

In the harmonic approximation, the mean extension has the simple form

$$\left\langle\frac{z}{L}\right\rangle = \frac{1}{L}\frac{\mathrm{d}}{\mathrm{d}\tilde{f}}\ln\mathcal{Z} = 1 - \frac{1}{2}\sum_p\langle|\alpha_p|^2\rangle + \cdots. \tag{50}$$

We define $D(p) \equiv L\langle|\alpha_p|^2\rangle$ and compute this two-point correlator perturbatively.

The unperturbed $D_0(p)$ is obtained via equipartition, or equivalently by performing the Gaussian (harmonic approximation) functional integral over α_p and α_p^* in ξ_0, yielding

$$D_0(p) = L\langle|\alpha_p|^2\rangle_0 = \frac{2}{\bar{A}(p^2 - 2q_0p) + \tilde{f}}, \tag{51}$$

26

where

$$q_0 = \left(C' - \frac{2G^2}{A'_2} \right) \frac{\omega\sigma}{2\bar{A}}.$$ (52)

The next step in determining $D(p)$ is to calculate the first two corrections, $\Pi_1(p)$ and $\Pi_2(p)$, induced by ξ_1 and ξ_2 respectively. We define these as lowest-order corrections to the full two-point function: $D(p) \equiv D_0(p)[1 + D_0(p)(\Pi_1(p) + \Pi_2(p))]$. Start by expanding the contribution $e^{-\xi_2}$ to the Boltzmann factor. There is no first order correction, so we go to second order:

$$
\begin{aligned}
\Pi_2(p) &= p^2 \frac{(\hat{A}(2\omega - p) + G\omega\zeta)^2}{\bar{A}((2\omega - p)^2 - 2q_0(2\omega - p) + \tilde{f})} \\
&\approx p^2 \frac{\hat{A}^2 + \zeta\hat{A}G}{\bar{A}}.
\end{aligned}
$$ (53)

The second correction arises from the expansion of the energy in powers of ξ_1. Once again we go to second order:

$$\Pi_1(p) = \frac{(G^2 p^2 + 2G\zeta(A'_1 p^2 - C'\omega p))}{2C'}.$$ (54)

As mentioned above, we have dropped terms of order σ^2 and higher: only odd-power terms will create chiral corrections to the extension curve, and we content ourselves with investigating the linear ones only. Putting the results of (54) and (53) together gives the propagator

$$D(p) = \left[D_0(p)^{-1} - \Pi_1(p) - \Pi_2(p) \right]^{-1}.$$ (55)

To get (55) we summed chains of Gaussian graphs, similarly to the random-phase approximation in many-body theory.

The relative extension can now be computed from (50):

$$
\begin{aligned}
\left\langle \frac{z}{L} \right\rangle &= 1 - \frac{1}{2L} \sum_p D(p) \\
&= 1 - \frac{1}{4\pi} \int_{-\infty}^{\infty} dp\, D(p) \\
&= 1 - \frac{1}{2} \left(A\tilde{f}(1 + F\sigma) \right)^{-1/2}.
\end{aligned}
$$ (56)

In this formula we have identified $A \equiv \bar{A} - 2\hat{A}^2/\bar{A} - G^2/C'$ as the *effective bend constant,* coarse-grained over a helix turn. (Had we kept $\mathcal{O}(\sigma^2)$ terms we could have made a similar identification of the coarse-grained twist constant C in terms of $\bar{A}, \hat{A}, C', G$.) We also defined

$$F \equiv \frac{2G^2}{A'_2 A} \left(\frac{\hat{A}}{\bar{A}} + \frac{A'_1}{C'} \right)$$ (57)

27

The key observation is now simply that F in (57) is *positive*.

Thus we have found a *chiral entropic elasticity* effect: the formulæ of the main text for $1 - z/L$ get multiplied by the asymmetric correction factor $(1 - F\sigma/2)$. (This analysis corrects an erroneous claim[42] that no such factor exists.)

The dependence of this chiral contribution to z/L on the stretching tension is different from the intrinsic twist-stretch term introduced in the main text, equation (41), and so in principle the two effects could be disentangled by fitting to data. In practice, however, the chiral effect in Figure 1 is too small to make any definite statement. Instead we tried eliminating the D term in (41) and replacing it by the F term in (56), which yields an equally good fit but with $F = -1.6$. Since this value is not positive, contrary to the prediction in (57), we conclude that the twist-stretch coupling D is needed to explain the asymmetry of the experimental data. This conclusion is qualitatively consistent with an earlier analysis[42] of the highest-force data; here the chiral entropic effect is very small (see (56)). Encouragingly, the fit values of A, C are similar to those quoted in the main text — our measurement of C is not sensitive to the precise mechanism of chiral symmetry breaking.

Appendix B: Domain of validity

In this appendix we endeavor to justify our perturbative approach to torsional directed walks, and in particular establish its domain of validity and hence the subset of the experimental data which falls into that domain.

Tunneling

As we have mentioned several times, the Schrödinger-type equation defined by (29) suffers from a singularity at the antipode $\theta = \pi$. Indeed, the operator $\mathcal{H}$ has no eigenstates at all. We have emphasized that this singularity is caused by our unphysical omission of self-avoidance effects, but it is still necessary to have some criterion for when the details of the nonlocal interaction correcting the problem will be unimportant, and some practical scheme for calculating in this regime.[58, 59, 60]

The key point to note is that if we let $t \equiv \tau^2/4$ and imagine solving our problem for *negative* (unphysical) values of t, then our problem disappears. Analytically continuing the ground-state eigenvalue in the complex t-plane back to positive (physical) t yields a result which is finite but no longer real: for small t its imaginary part gives the probability of a rare *barrier penetration* process. The real part is an approximate eigenvalue describing the metastable state and controlling the intermediate asymptotics

of Ψ: this is the number we seek. When the imaginary part is small, the real part can be obtained from the lowest orders of perturbation theory, even though eventually at high orders the series diverges.

We can estimate the imaginary part of the eigenvalue by finding the saddle point (or "instanton" or "bounce" or "domain wall" solution) of the functional integral giving rise to (29). This is the function $\theta(s)$ satisfying the ordinary differential equation $A^2\ddot{\theta} = dV/d\theta$, where $V(\theta) \equiv (1 - \cos\theta)(K^2 - t(1 - \cos\theta)/(1 + \cos\theta))$. The elastic energy of this configuration is then given by

$$\frac{\bar{E}}{k_{\mathrm{B}}T} = 2\int_0^{\theta_1} \mathrm{d}s\Big[\frac{A}{2}\dot{\theta}^2 + \frac{1}{A}V(\theta)\Big] = 2\int_0^{\theta_1} \mathrm{d}\theta\sqrt{2V}, \tag{58}$$

where θ_1 is the "turning point", where $V(\theta_1) = 0$. The imaginary part of the analytically-continued eigenvalue is then proportional to $\mathrm{e}^{-\bar{E}/k_{\mathrm{B}}T}$. Numerical evaluation shows that this factor is smaller than 0.02 when $t < 0.6(A\tilde{f} - 1.6)$, and we have imposed this as one of the conditions selecting the data points used in Figure 1.

Perturbation theory

From the previous subsection and the references cited there we know that when the tunneling criterion is satisfied perturbation theory will be an asymptotic expansion, which we may approximate by its first terms. In this subsection we will quote the eigenvalues of (31) obtained using second-order perturbation theory. In the last term we expand $\rho^4/(1 - \rho^2/4)$ in power series, since each succeeding term is formally suppressed by a power of K^{-1}; we keep the terms $\rho^4 + \rho^6/4$. We again abbreviate $t \equiv \tilde{\tau}^2/4$.

Using the operator notation of the main text, we find $\mathcal{H} = \mathcal{H}_0 + \delta\mathcal{H}$, where $\mathcal{H}_0$ is the first line of (33) and

$$\begin{aligned}
\delta\mathcal{H} = \frac{1}{8A}\Big[&-\frac{t}{32K^3}(\mathcal{A}_+{}^6 + 3\mathcal{A}_+{}^2\mathcal{B}_+{}^4 + 3\mathcal{A}_+{}^2\mathcal{B}_+{}^4 + \mathcal{B}_+{}^6) \\
&+\frac{1}{4}\Big(1 - \frac{t}{K^2} - \frac{9t}{4K^3}\Big)(\mathcal{A}_+{}^4 + 2\mathcal{A}_+{}^2\mathcal{B}_+{}^2 + \mathcal{B}_+{}^4) \\
&-t\Big(\frac{2}{K^2} + \frac{9}{4K^3}\Big)(\mathcal{A}_+{}^2 + \mathcal{B}_+{}^2) - 2\Big(1 + \frac{t}{K^2} + \frac{3t}{4K^3}\Big)\Big], \tag{59}
\end{aligned}$$

plus terms annihilating the perturbative ground state. From this we compute zeroth through second-order shift:

$$\begin{aligned}
\mathcal{E} &= -\tilde{f} - \frac{2t}{C} + \frac{K}{A}\Big(W_1 - \frac{t}{4K^3}W_2 - \Big(\frac{t}{4K^3}\Big)^2 W_3\Big) \quad \text{where} \\
W_1 &= 1 - \frac{1}{4K} - \frac{1}{64K^2}
\end{aligned}$$

29

$$W_2 = 1 + \frac{5}{8K} - \frac{9}{32K^2}$$
$$W_3 = \frac{9}{4}(1 + \frac{5}{2K} + \frac{16}{9K^2}). \tag{60}$$

Taking thermodynamic derivatives as in the text (see (16)), and recalling $t \equiv \tilde{\tau}^2/4$, gives

$$\omega_0 \sigma = \tilde{\tau}\left[\frac{1}{C} + \frac{1}{4AK}\left(1 + \frac{1}{2K} + \frac{21}{64K^2} + \frac{\tilde{\tau}^2}{16K^3}(2 + \frac{15}{8K} + \frac{9}{8K^2}) + M\right)\right]$$
$$z/L = 1 - \frac{1}{2K}\left(1 + \frac{1}{64K^2} + \frac{\tilde{\tau}^2}{16K^3}(2 + \frac{15}{8K} - \frac{9}{8K^2}) + M\right), \tag{61}$$

where

$$M = \left(\frac{\tilde{\tau}^2}{16K^3}\right)^2 \left(\frac{9}{4}\right)\left(5 + \frac{15}{K} + \frac{112}{9K^2}\right). \tag{62}$$

The corrections for kinks, (39) and (40), and the other corrections in (41) must be added to the expressions (61). The resulting formulæ are the ones actually used in the fit shown in Figure 1.

We are now in a position to state the conditions for perturbation theory to be useful. Our expansion is in powers of K^{-1} and $\tilde{\tau}^2/16K^3$, so both of these must be small. To be more precise, we imagine holding the force $\tilde{f}$ fixed while varying the torque $\tilde{\tau}$, as in the experiment. The coefficient of $\tilde{\tau}^2$ in z/L then gives the information we need to obtain the twist stiffness. Comparing the highest-order term of this coefficient retained above to the leading term, we find their ratio to be less than 10% when $K^2 > 3$. This explains another of the cuts made on the data in the text. We should also require that $\tilde{\tau}^2/16K^3$ be small, but this is automatically satisfied when the other imposed conditions are.

Acknowledgments

References

[1] Doi, M.; Edwards, S.F. *The Theory of Polymer Dynamics.* Clarendon Press: Oxford, 1986.

[2] Kamien, R.D. *Eur. Phys. J. B* **1998**, 1, 1–4.

[3] Goldstein, R.E.; Powers, T.R.; Wiggins, C.H. *Phys. Rev. Lett.* **1998** (in press).

[4] Călugăreanu, G. *Rev. Math. Pures Appl.* **1959**, 4, 5–20.

[5] White, J.H. *Am. J. Math.***1969**, 91, 693–727.

[6] Fuller, F.B. *Proc. Nat. Acad. Sci. USA* **1978**, 75, 3557–3561.

[7] Smith, S.B.; Finzi, L.; Bustamante, C. *Science* **1992**, 258, 1122–1126.

[8] Schurr, J.M.; Smith, S.B. *Biopolymers* **1990**, 29, 1161–1165.

[9] Perkins, T.T.; Smith, D.E.; Larson, R.G.; Chu, S. *Science* **1995** 268, 83–87.

[10] Wang, M.D.; Yin, H.; Landick, R.; Gelles, J.; Block, S.M. *Biophys. J.* **1997**, 72,1335–1346.

[11] Bustamante, C.; Marko, J.F.; Siggia, E.D.; Smith, S. *Science* **1994**, 265, 1599–1600.

[12] Marko, J.F.; Siggia, E.D. *Macromolecules* **1995**, 28, 8759–8770.

[13] Vologodskii, A. *Macromolecules* **1994**, 27, 5623–5625.

[14] Strick, T.R.; Allemand, J.-F.; Bensimon, D.; Bensimon, A.; Croquette, V. *Science* **1996**, 271, 1835.

[15] Strick, T.R.; Allemand, J.-F.; Bensimon, D.; Croquette, V. *Biophys. J.* **1998** (in press).

[16] Allemand, J.-F.; Croquette, V. Unpublished **1997**.

[17] Marko, J.F.; Siggia, E.D. *Phys. Rev.* **1995**, E52, 2912–2938.

[18] Nelson, P. New measurements of DNA twist elasticity. *Biophys. J.* **1998**, 74, 2501–2503. (Proceedings of Joint DIMACS/PMMB/MBBC Workshop on DNA Topology, April 1997).

[19] Moroz, J.D.; Nelson, P. *Proc. Nat. Acad. Sci. USA* **1997**, 94, 14418–14422.

[20] Bouchiat, C.; Mézard, M. *Phys. Rev. Lett.* **1998**, 80, 1556–1559.

[21] Vologodskii, A.V.; Marko, J.F. *Biophys. J.* **1997**, 73, 123–132.

[22] Marko, J.F. *Europhys. Lett.* **1997**, 38, 183–188.

[23] Marko, J.F. *Phys. Rev.* **1998**, E57, 2134–2149.

[24] Shimada, J.; Yamakawa, H. *Macromolecules* **1984**, 17, 689–698.

[25] Love, A.E.H. *Treatise on the mathematical theory of elasticity.* Cambridge: Cambridge University Press, 1906.

[26] Cluzel P.; Lebrun, A.; Heller, C.; Lavery, R.; Viovy, J.-L.; Chatenay, D.; Caron, F. *Science* **1996**, 271, 792–794.

[27] Marko, J.F.; Siggia, E.D. *Macromolecules* **1994**, 27, 981–988. Erratum *Ibid.* **1996**, 29, 4820.

[28] Landau, L.D.; Lifschitz, E.M. *Theory of Elasticity.* London: Pergamon Press, 1986.

[29] Kirchoff, G. *J. Reine. Angew. Math. (Crelle)* **1859**, 50, 285–313.

[30] Record, M.; Mazur, S.; Melancon, P.; Roe, J.; Shaner, S.; Unger, L. *Ann. Rev. Biochem.* **1981**, 50, 997–1024.

[31] Shore, D.; Baldwin, R.L. *J. Mol. Biol.* **1983**, 170, 957–981.

[32] Taylor, W.H.; Hagerman, P.J. *J. Mol. Biol.* **1990**, 212, 363–376.

[33] Crothers, D.M.; Drak, J.; Kahn, J.D.; Levene, S.D. *Meth. Enzymology* **1992**, 212, 3–29.

[34] Shore, D.; Baldwin, R.L. *J. Mol. Biol.* **1983**, 170, 983–1007.

[35] Horowitz, D.A.; Wang, J.C. *J. Mol. Biol.* **1984**, 173, 75–91.

[36] Heath, P.J.; Clendenning, J.B.; Fujimoto, B.S.; Schurr, J.M. *J. Mol. Biol.* **1996**, 260, 718–730.

[37] Fujimoto, B.S.; Schurr, J.M. *Nature* **1990**, 344, 175–178.

[38] Schurr, J.M.; Fujimoto, B.S.; Wu, P.; Song, L. In *Topics in Fluorescence Spectroscopy*, volume 3; Lakowicz, J.R. Ed.; Plenum Press: New York, 1987, 137–229.

[39] Hagerman, P.G. *Ann. Rev. Biophys. Biophys. Chem.* **1988**, 17, 265–286.

[40] Fuller, F.B. *Proc. Nat. Acad. Sci. USA* **1971**, 68, 815.

[41] Fain, B.; Rudnick, J.; Östlund, S. *Phys. Rev.* **1997**, E55, 7364–7368.

[42] Kamien, R.D.; Lubensky, T.C.; Nelson, P.; O'Hern, C.S. *Europhys. Lett.* **1997**, 38, 237–242.

[43] O'Hern, C.S.; Kamien, R.D.; Lubensky, T.C.; Nelson, P. *Euro. Phys. J.* **1998**, B1, 95–102.

[44] Ulyanov, N.B.; Zhurkin, V.B. *J. Biomol. Struct. Dyn.* **1984**, 2, 361–385.

[45] Srinivasan, A.R.; Torres, R.; Clark, W.; Olson, W.K. *J. Biomol. Struct. Dyn.* **1987**, 5, 459–496.

[46] Sarai, A.; Mazur, J.; Nussinov, R.; Jernigan, R.L. *Biochemistry* **1989**, 28, 7842–7849.

[47] Trifonov, E.N.; Tan, R.K.-Z.; Harvey, S.C. In *DNA bending and curvature*; Olson, W.K., Sarma, H., Sundaralingam, M. Eds.; Adenine Press: Schenectady, 1987, 243–254.

[48] Schellman, J.A.; Harvey, S.C. *Biophys. Chem.* **1995**, 55, 95–114.

[49] Bensimon, D.; Dohmi, D.; Mézard, M. *Europhys. Lett.* **1998**, 42, 97–102.

[50] Nelson, P. *Phys. Rev. Lett.* **1998** (in press).

[51] Feynman, R.P.; Hibbs, A.R. *Quantum Mechanics and Path Integrals*. McGraw-Hill: New York, 1965.

[52] Tung, Wu-ki. *Group Theory in Physics*. World Scientific: Signapore, 1985.

[53] Landau, L.D.; Lifshitz, E.M. *Quantum mechanics*. Pergamon Press: London, 1977.

[54] Smith, S.; Cui, Y.; Bustamante, C. *Science* **1996**, 271, 795–799.

[55] Odijk, T. *Macromolecules* **1995**, 28, 7016–7018.

[56] Press, W.H. *Numerical Recipes*. Cambridge University Press: Cambridge, 1996.

[57] Moroz, J.D.; Kamien, R.D. *Nucl. Phys. B* **1997**, 506, 695–710.

[58] Langer, J. Theory of the condensation point. *Ann. Phys.*, **1967**, 41, 108–157.

[59] Zinn-Justin, J. The principles of instanton calculus. In Zuber, J.-B., Stora, R. Eds. *Recent advances in field theory and statistical mechanics.* Amsterdam: North-Holland, 1984, 39–172. North-Holland.

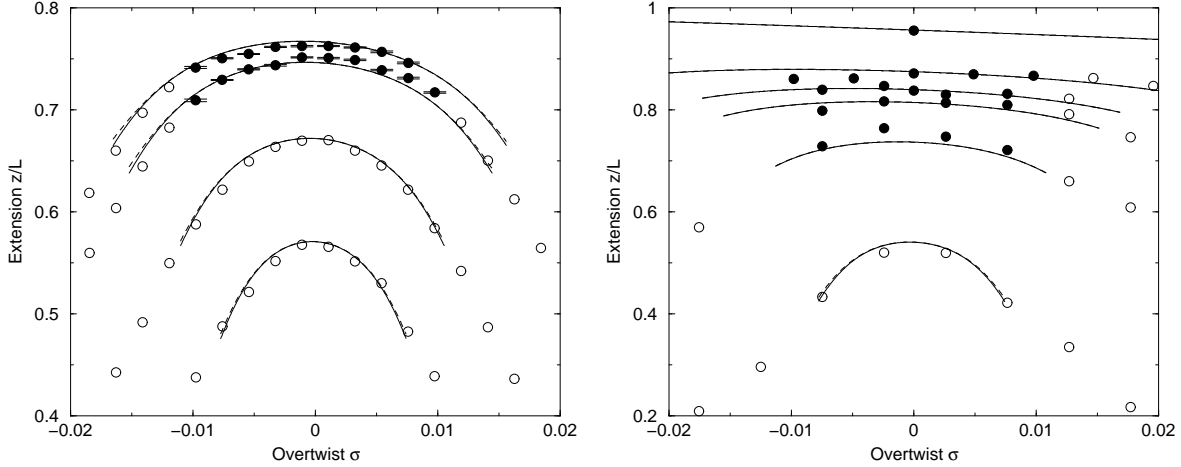[60] Coleman, S. *Aspects of symmetry.* Cambridge: Cambridge University Press, 1985.

Figure 1: Relative extension of λ-DNA versus applied force f and overtwist σ: a single global fit to two experiments. Fitting our model to the solid points shown correctly predicts many of the open symbols shown, even though they were not used in the fit. On the left are experimental data from Allemand and Croquette:[16] from top to bottom, the curves are at fixed force 0.388, 0.328, 0.197, and 0.116 pN. The error bars reflect the measurement of extension; estimated errors in the determination of the force are not shown. On the right are data from Strick *et al.*:[14] from top to bottom, the curves are at fixed force 8.0, 1.3, 0.8, 0.6, 0.3, and 0.1 pN (error estimates not available). Points corresponding to f, σ where the DNA is known to denature or undergo structural change have been omitted from the right hand graph. Solid symbols are within the range of validity of our model (for example, all solid symbols have $K^2 > 3$, see text); open symbols were not included in the fit. A total of 69 experimental data points were used in the fitting procedure. Some of these points are not shown; they had force not equal to one of the ten values listed above. The solid lines are a single global fit to both datasets using the theory developed in the text (see (41)). The dashed (higher) lines are the same theoretical curves but without our estimated non-perturbative contribution (section V.D).
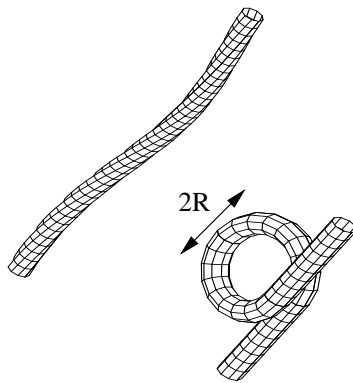
Figure 2: Diagram showing the idealized circular loop model of a plectoneme. The twisted and slightly writhed conformation above is shortened by the coil circumference as the plectoneme forms.